Analytic and Experimental Investigation of Three-Winglet "Louvered" Planforms[1]

David S. Miklosovic[2]
United States Naval Academy, Annapolis, Maryland, 21402-5042

An analytic and experimental effort was undertaken to assess the performance enhancements of three winglets mounted chordwise to the tip of a rectangular wing. Three configurations of "louvered" arrangements were analyzed with a vortex lattice method and tested in a low-speed wind tunnel at a Reynolds number of 600,000. The analytic method provided good predicted trends in lift, drag, and (to a lesser degree) pitching moment. The experimental results showed that the winglets increased the lift coefficient as much as 41% at the same angle of attack, decreased the drag coefficient as much as 44% at the same lift coefficient, and improved the peak L/D by up to 11%. The results suggest that multiple winglet dihedral variations might be used as actively-controlled surfaces to improve aircraft performance at various flight conditions.

I. Nomenclature

a	=	lift curve slope, $dC_L/d\alpha$
AR	=	wing aspect ratio, b^2/S
b	=	wing span
c	=	wing chord length
C	=	test section cross-sectional area
C_d , C_D	=	section/wing drag coefficient
C_ℓ , C_L	=	section/wing lift coefficient
C_m , C_M	=	wing pitching moment coefficient
D	=	drag force
e	=	span efficiency factor
L	=	lift force
LE	=	leading edge
M	=	pitching moment
n_{crit}	=	log of the boundary layer amplification factor
q	=	freestream dynamic pressure, $\left(\rho U_\infty^2\right)/2$
Re_c	=	Reynolds number, $\left(\rho U_\infty c\right)/\mu$
S	=	wing planform area, $b\bar{c}$
TE	=	trailing edge
u	=	axial velocity increment
U	=	steady-state axial velocity
v	=	spanwise velocity component
w	=	downwash velocity component
x	=	wing coordinate in the chordwise direction
y	=	wing coordinate in the spanwise direction
z	=	vertical coordinate

Greek

α	=	geometric angle of attack (AOA)
γ	=	winglet dihedral angle
ε	=	downwash angle
Γ	=	circulation
ξ	=	vorticity
μ	=	dynamic viscosity
ρ	=	fluid density

Subscripts

0	=	wing zero-lift condition
$1,2,3$	=	winglet number, indexed fore to aft
∞	=	freestream condition
AC	=	referenced to the wing aerodynamic center
$c/4$	=	referenced to the wing quarter-chord position
ref	=	based on reference characteristic (i.e., baseline)
w	=	characteristic of a winglet

II. Introduction

Winglets have long been recognized for marked reductions in induced drag, which yields improved L/D, extended range, and reduced fuel burn [1, 2]. These devices improve performance by altering the spanwise loading of the planform, thus altering the downwash distribution behind the wing and reducing the induced drag. The drag reduction that results from winglets is most commonly attributed to the increase in the effective aspect ratio, AR, of the planform. As such, this effect makes the most impact at high-lift conditions for an aircraft; namely takeoff, landing, and maneuvering flight.

A. Background

Winglet design has typically focused on the so-called "crossover point" on the drag polar, or the point at which the drag benefits overcome the drag penalties of the winglet configuration. While the added length of the winglet contributes to increasing the effective span of the wing (thus reducing lift-induced contributions to drag), the additional area and junction with the wing increases parasite drag through additional friction and interference drag. Thus, a wing will demonstrate an overall drag reduction if it operates below the crossover velocity. Maughmer [3] showed that winglets increased overall sailplane wing performance over much of its operating range, improving the glide ratio and sink rate as much as 10%. Whitcomb's wind tunnel work with winglets on a narrow-body jet transport [4] showed an improvement in lift-to-drag ratio of 9%, more than twice the improvement from using an equivalent planar wingtip extension. Winglet configurations optimized to include viscous effects were shown by Chattot [5] to vary little from inviscid design methods, which suggests that potential-flow lifting line and vortex lattice analyses can yield useful, if not comprehensive, results for multiple lifting-surface planforms in the linear aerodynamic regime.

[1] Adapted from Miklosovic, D. S., 2007, "Analytic and Experimental Investigation of Dihedral Configurations of Three-Winglet Planforms," submitted for publication to ASME Journal of Fluids Engineering, Am. Soc. of Mechanical Engineers.
[2] Assistant Professor, Aerospace Engineering Department.

Multiple lifting-surface planforms have demonstrated benefits at low Reynolds numbers as well. For Re = 160,000–300,000, an increase in L/D of 15–30% was measured by adding five flat-plate winglets to a rectangular baseline wing [6]. A substantial increase in lift curve slope was noted and it was attributed to the dihedral spread of winglets at a zero local incidence. Furthermore, the percent increase exceeded the planform area added by the winglets. Work done by Kroo [7] on nonplanar lifting systems has shown that the shape of the wake, rather than the shape of the wing, has the largest impact on induced drag for a given lifting condition. A split-tip configuration he studied computationally and experimentally showed a 13–15% increase in span efficiency (e = 1.11) compared to an elliptic planar wing. The optimized "C" wing configuration produced e = 1.46, suggesting that nonplanar distributions in the circulation can lead to drag reduction.

B. Supporting Theory

The wing aerodynamic coefficients of lift, C_L, drag, C_D, and pitching moment, C_M, are defined in equations (1), (2), and (3), respectively. In these equations, the aerodynamic loads (L, D, and M) are non-dimensionalized by the freestream dynamic pressure, q, and the wing reference planform area, S_{ref}. The moment coefficient requires an additional length scale of the reference chord length, c_{ref}.

$$C_L = \frac{L}{qS_{ref}} \tag{1}$$

$$C_D = \frac{D}{qS_{ref}} \tag{2}$$

$$C_M = \frac{M}{qS_{ref}c_{ref}} \tag{3}$$

To determine the relative loading of a lifting planform, the spanwise variation in the span load coefficient is determined The span load coefficient is defined in Eqn. (4). C_ℓ represents the local effective 2D value of the lift coefficient, while C_L represents the wing overall lift coefficient.

$$SL\ Coef = \frac{C_\ell\, c}{C_L\, \bar{c}} \tag{4}$$

The winglets are not necessarily at the same angle of attack (AOA) as the wing. The effective AOA of a winglet, $\alpha_{w,eff}$, is determined by a coordinate transformation through a local dihedral rotation then a pitch rotation and is given in Eqn. (5).

$$\alpha_{w,eff} = \frac{\pi}{2} - \cos^{-1}\left(\sin\alpha\cos\gamma\right) \tag{5}$$

C. Purpose

The present study was undertaken to study three independent, articulated winglets on a symmetrical half-span wing model to gain a better understanding of the aerodynamic effects of manipulating multiple winglets in flight. This work focused on the effect of dihedral configurations, and analytic results supported wind tunnel force measurements. The performance enhancements were quantified in terms of the lift curves, drag polars, and spanload distributions of the configurations.

III. Experimental and Analytic Details

A. Facility and Models

The wind tunnel tests were performed in the former Closed-Circuit Wind Tunnel (CCWT) at the United States Naval Academy. The CCWT was a low speed, subsonic wind tunnel with a 137×97 cm test section. Testing was conducted at near-atmospheric pressures, at effective Reynolds numbers of 579,000–603,000.

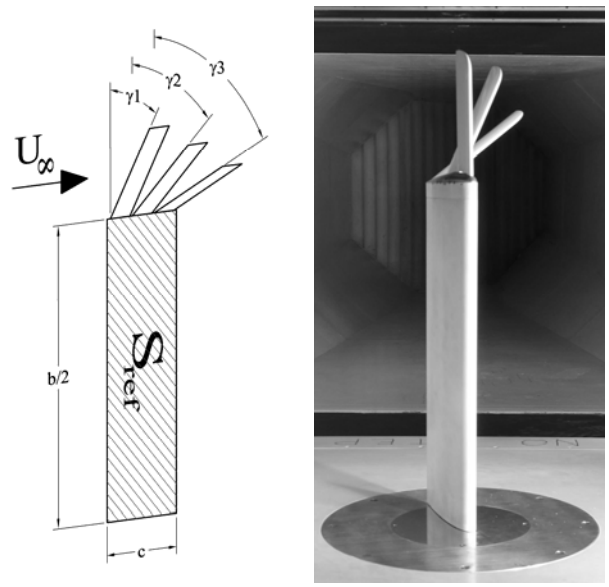

a) Geometry definition **b) Configuration 0/30/60**

Figure 1. Multiple winglet geometry

The baseline semi-span wing had a constant NACA 0018 airfoil section [8] with a 55.9 cm halfspan and a 17.8 cm chord. Thus, the effective aspect ratio was 6.29 for a projected fullspan wing model. The baseline wing, with the winglets removed, had a rounded tip with an NACA 0018 profile. This geometry, along with the comparatively large LE radius of the section, promoted effective side- and leading-edge suction to affect the induced drag. Added to the tip of the baseline wing were three individual winglets which approximate an NACA 0015 section [8]. The winglets are numbered fore-to-aft for the purpose of quantifying the dihedral configuration in the format of $\gamma_1/\gamma_2/\gamma_3$, as shown in Figure 1a. Each winglet had a span of 20.3 cm and a chord of 5.0 cm with an aspect ratio of 4.6. The winglets were each capable of adjustment through ±90 deg local dihedral angle as well as ±90 deg local pitch angle (rotating about the winglet quarter chord). Figure 1b shows the "0/30/60" configuration.

B. Force Measurements and Procedure

The semi-span wing model was offset 1.8 mm above a splitter plate mounted 5.72 cm above the tunnel floor, with a carry-through structure to the balance installed beneath the test section. Aerodynamic loads were measured with a six-component compact platform balance. The measurement uncertainty of these force measurements was established by repetitive testing at a fixed flow condition. This was done at 11 deg AOA over the acquisition of 20 consecutive datasets at Reynolds numbers of 200,000–700,000. The mean and uncertainty in the measurements were calculated using standard

error analyses [9] and are shown in Table 1. In particular, the wing coefficients have shown a maximum 1σ uncertainty of 0.0024 in C_L (0.3%), 0.0011 in C_D (2.3%), and 0.0017 in $C_{M_{c/4}}$ (11.8%) at the targeted Reynolds number.

Table 1. Measurement uncertainty: Baseline model

Mean Value ± 1σ Error			
Re_c	C_L	C_D	$C_{M_{c/4}}$
195,300 ±171	0.819±0.003	0.0584±0.0013	0.0047±0.0011
398,100 ±450	0.812±0.002	0.0505±0.0009	0.0100±0.0014
581,400 ±1,386	0.806±0.002	0.0485±0.0011	0.0144±0.0017
722,500 ±3,423	0.805±0.003	0.0478±0.0013	0.0161±0.0013

The targeted Reynolds number was (nominally) 600,000. For each winglet configuration, the model was pitched through an alpha sweep of –2 to +24 deg in 1 deg increments using the pitch-pause technique. During data acquisition, nine channels were scanned (six balance outputs, the balance excitation voltage, the test section dynamic pressure, and the freestream air temperature) at 6.5-digit precision over an integration aperture of 20 power line cycles. Reynolds number stability was maintained at ±50,000 of the target condition. This procedure generally limited the freestream temperature to no more than 46 deg C.

To affect equivalencies in comparison of the non-dimensional coefficients, the reference area of the baseline wing was used in calculations of C_L, C_D, and C_M for all winglet configurations. Additionally, the baseline chord length was used for all Reynolds number calculations.

All force and moment measurements were corrected for wind tunnel wall interference effects. These included buoyancy, solid and wake blockage (single-pass Maskell method for separated flow), streamline curvature corrections, and downwash corrections as prescribed by common practice [10]. The semi-span models had a low frontal-area blockage of 4% (and a planform-to-tunnel-cross-section ratio of $S/C = 0.077$) and a span ratio of 54%. Thus, the pre-stall corrections created at most a 0.46 deg increase in AOA, a decrease in C_L of 0.016 or less, an increase in C_D of 0.0069 or less, and a change in C_M of less than 0.0006. The effective velocity through the test section was increased by 3% at 25 deg AOA as a result of solid and wake blockage effects.

C. Analytic Approaches

Analytic results were generated using two well-documented codes. The low-Reynolds number airfoil performance was benchmarked using the XFOIL code. XFOIL is used for design and analysis for low Reynolds number airfoils and employs a high-order panel method with a fully-coupled viscous/inviscid interaction method. The free transition criterion (specifically, the $e^{n_{crit}}$ criterion) was used for the viscous calculations, where n_{crit} is the log of the amplification factor of the most-amplified frequency which triggers transition. The present study used $n_{crit} = 7$ (corresponding to a 0.161% turbulence level, the approximate the turbulence intensity of the CCWT). It should be noted that the assumptions for this transition criterion (no cross flow instabilities, attachment-line transition, or bypass transition) are met for the present 2D analysis [11]. Most computed cases for $\alpha < \alpha_{stall}$ converged within about a dozen iterations.

For 3D planform characteristics, the Vortex Lattice Method (VLM) of Margason, Lamar, and Herbert [12] was applied. VLM is an extension of the finite step lifting-line theory, which assumes steady, irrotational, inviscid, attached flow. These calculations were performed assuming full leading edge (LE) suction and side edge attached flow. The multiple-winglet configurations were modeled using three combined planforms and 270 horseshoe vortices: a 15×11 array (chordwise × spanwise) on the main wing and a 5×7 array on each winglet. VLM trade studies were performed to ascertain trends which were validated through wind tunnel testing. Furthermore, the VLM analysis enabled a detailed examination of span loading and flowfield distributions (velocity, vorticity, and downwash) that weren't available at the time of the experimentation.

IV. Results

Results are presented for the semi-span wing with and without three winglets. The primary value of these results lies in the comparisons at varying local dihedral angle configurations to wings without winglets to gain a perspective on the advantages and disadvantages of utilizing these types of configurations. In light of this comparison, all coefficients are based on the reference area of the baseline wing. This enables direct comparison of the aerodynamic forces produced by diverse configurations. The presented results focus on the analysis of the airfoil performance, the baseline wing performance, the performance of the "louvered" winglet configurations, and a wake analysis of the configurations considered.

A. Airfoil Section Analysis

The 2D analytic results for the NACA airfoils benchmarked the sectional characteristics, and were used to ascertain the magnitude of the Reynolds number effects. With the baseline wing section (18% thick) operating at a Reynolds number of 600,000, the winglet sections (15% thick) were operating at a Reynolds number of 170,000. Therefore, differences in the airfoil performance were manifest as thickness and Reynolds effects. From the lift curves in Figure 2a, the baseline section encountered a laminar separation bubble, which created the change in lift slope at around 10 deg AOA. However, the winglet section exhibited the classic leading edge stall characteristic at about 13 deg AOA. The main conclusion of this analysis is that the winglet airfoils stalled 3 deg sooner than the baseline airfoil at an 11% lower $C_{\ell,max}$. More significantly, Figure 2b shows that the value of $C_{d,0}$ was 50% higher for the winglet airfoil sections, which had 82% laminar flow on the upper surface compared to 60% for the baseline wing section. Primarily due to increased pressure drag, this impacted the total contribution to parasite drag on a finite wing or a flight vehicle. This comparison emphasizes the trade-off involved at the crossover point: the reduction in induced drag at the cost of a higher overall parasite drag.

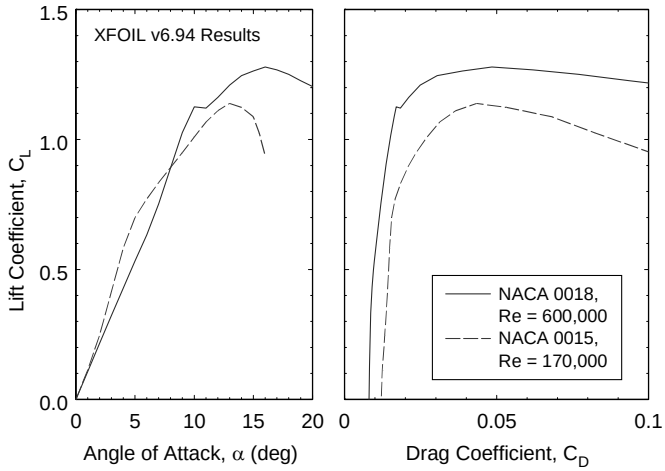

a) Lift Curve **b) Drag Polar**

Figure 2. XFOIL analysis of 2D airfoil sections used

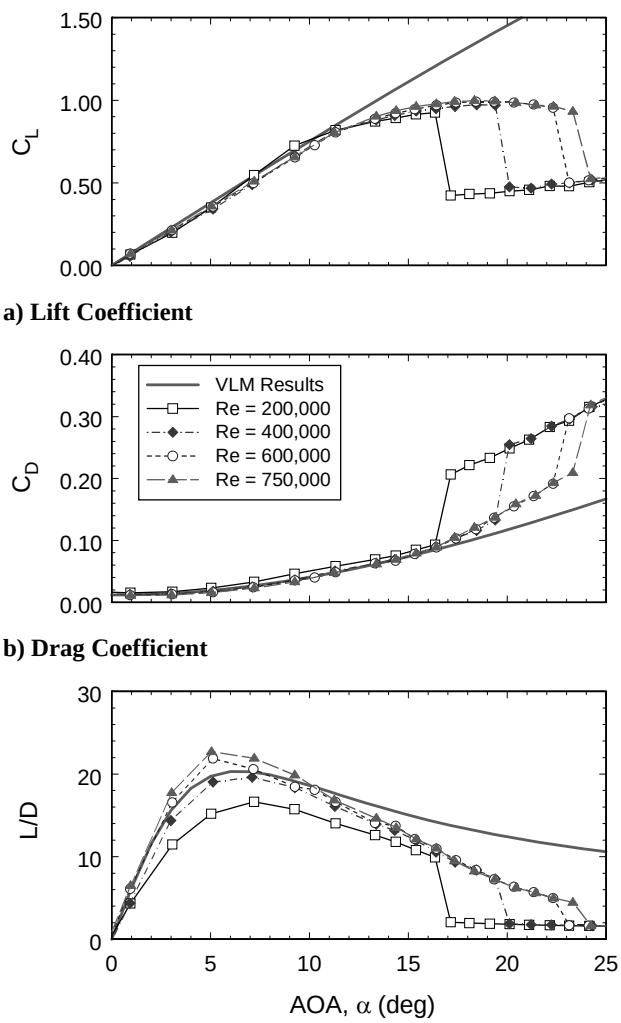

a) Lift Coefficient

b) Drag Coefficient

c) Lift-to-Drag ratio

Figure 3. Baseline wing Reynolds number sensitivity

B. Baseline Wing Performance

The rectangular baseline wing was used as the reference configuration when comparing the winglet configurations and was benchmarked against the VLM analysis. Full alpha sweeps were run at four different effective Reynolds numbers (200,000, 400,000, 600,000, and 750,000) to determine the sensitivity to the flow regime. The results in the linear regime show a good comparison with the VLM analysis, particularly the lift curves of Figure 3a. At a Reynolds number of 600,000, the baseline wing achieved a lift curve slope of 0.0704/deg, which was corroborated by the analysis. At this Reynolds number, stall occurred at $C_{L,max}$ = 0.991 at 18.4 deg AOA. As the Reynolds number increased from 200,000 to 750,000, the insipient stall AOA progressively increased from 16.4–23.3 deg.

The drag polars are shown in Figure 3b. For the analytic drag comparison, the $C_{D,i}$ values from the VLM code were offset by the experimental $C_{D,0}$ as obtained in the wind tunnel (0.0120). While this method is imprecise at the theoretical level, it is a common practice in benchmarking analytic and experimental results [13], and has been validated in other comparative studies by the author [14] to validate the drag polar shape factor. In practice, the amount of LE suction would not be 100% as in the VLM, but around 97% for the present wings, thereby creating a slightly steeper theoretical induced drag shape factor [15]. At a Reynolds number of 600,000, the baseline wing achieved a $C_{D,min}$ = 0.0116 and $(L/D)_{\max}$ = 21.9 at 5 deg AOA (refer to Figure 3c). The effect of increasing the Reynolds number was to decrease $C_{D,min}$ progressively from 0.0153–0.0113. Because of the observed sensitivity due to Reynolds number, the allowable Re variability was limited to ±50,000 for these tests.

C. "Louvered" Wing Lift Characteristics

The so-called "louvered" configurations indicated that all three winglets were adjusted to the same local dihedral angle, or $\gamma_1 = \gamma_2 = \gamma_3 = k$, where k corresponded to 0 and 45 deg. In the practical application of multiple winglets, the 0/0/0 configuration is a valid "winglet-on" reference geometry. In this case, the addition of the winglets added 30% to the true planform area and 43% to the true aspect ratio of the base wing.

The experimental lift results (shown in Figure 4a) showed that the 45/45/45 configuration was limited to a 34% increase in the lift slope over 0–10 deg AOA, while the 0/0/0 configuration showed a 41% increase. The VLM analysis predicted these increases to be 40% and 46%, respectively, in the linear regime. Prandtl's work [16] originally predicted that the change in the lift slope over the linear region can be expressed as an AR effect. This is evident in the 0/0/0 configuration, which had the largest physical span and the highest effective AR (9.01), and yielded the highest lift slope of 0.100/deg. Despite the varying lift slopes, the stall point remained relatively unchanged (21–22 deg AOA). It should be noted here that the lift increments at the same geometric AOA for the 0/0/0 configuration in the linear regime were in excess of those expected by the addition of the winglet planform area (which would increase C_L 30%), and the increase in the aspect ratio (which would increase C_L another 8% for an elliptic span loading). The experimental results also showed a 17–25% increase in C_L from 10 deg to the stall AOA, increasing $C_{L,max}$ 12–24% for the louvered configurations.

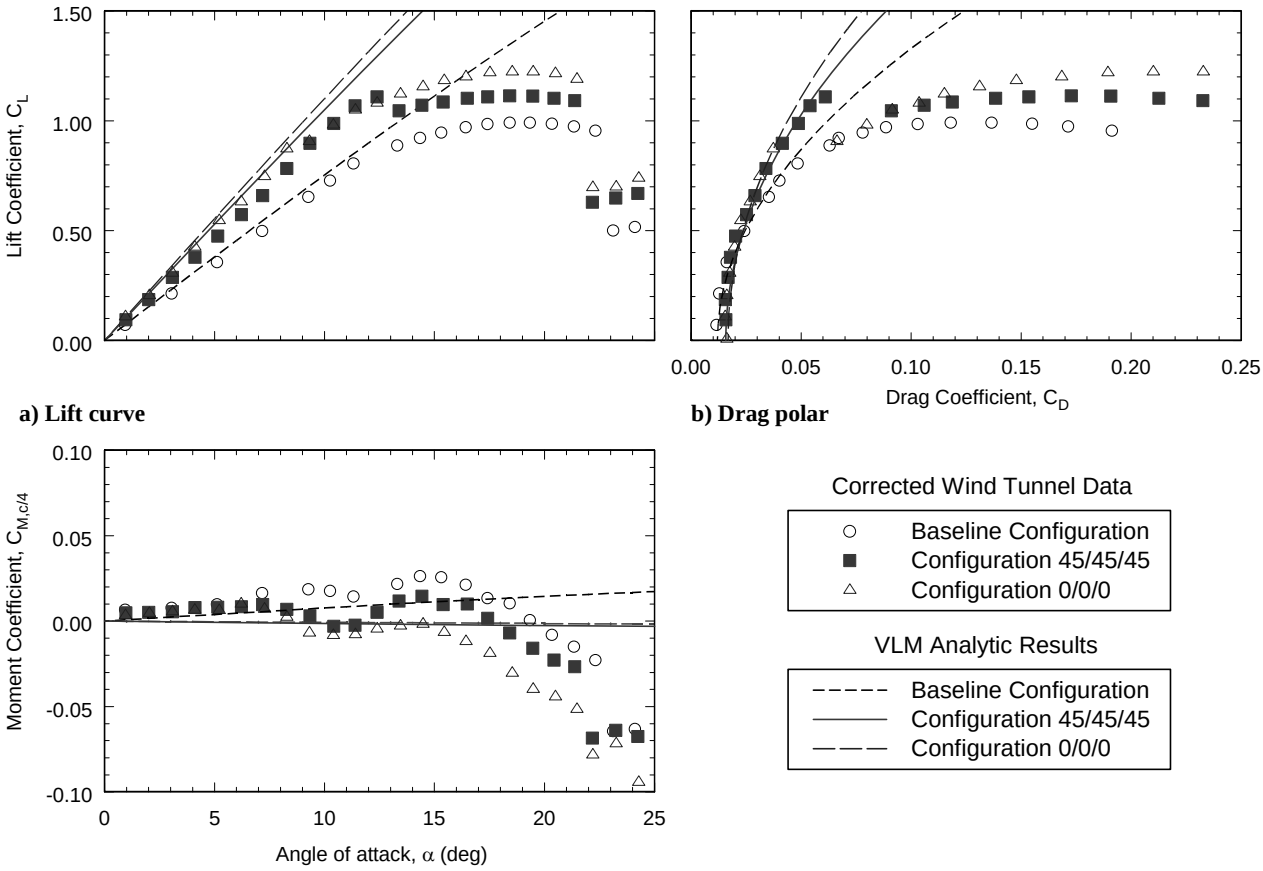

Figure 4. Louvered-wing experimental and analytic results

D. "Louvered" Wing Drag Characteristics

The drag polars of Figure 4b show that $C_{D,0}$ increased by 32% with the addition of either louvered configuration, the result of added parasite drag due to Reynolds effects on the winglets plus the added interference between the four lifting surfaces. Both louvered configurations yielded the same value of $C_{D,0}$ (0.0163) within the experimental uncertainty.

This also resulted in similar-magnitude drag increases at the equivalent geometric AOA as the baseline model, a magnitude that is consistent with the percent increase in true planform area. But in terms of C_D for a given C_L, there was a noteworthy crossover point in the drag polar at around C_L = 0.45. Below this point, the winglets produced more drag at the same lift. Above this point, however, the reductions in induced drag overcame the parasitic penalties. As an example, the overall drag reduction was 27–31% for the louvered configurations at C_L = 0.8, and as high as 44% for C_L = 0.95. These decrements were far beyond those expected by a pure aspect ratio effect, which would act to decrease C_D 17–22% for the louvered configurations, assuming an elliptic span loading. Therefore, the experimental drag reductions are beyond the oft-cited influences of additional planform area and aspect ratio.

A notable feature of these drag polars was that C_D abruptly increased at C_L = 1.1 for the 45/45/45 configuration and at C_L = 0.9 for the 0/0/0 configuration. This was caused by winglet #1 stalling due to its higher loading condition and the low-Reynolds effects present (this has been confirmed by a decrease in the $C_{M,c/4}$ in Figure 4c). The flow on the aft winglets remained attached due to the downwash from the upstream winglets.

As a result of the lift enhancements and drag reductions, the peak L/D ratio increased by 7–11%, (24.2–23.4). The improved L/D, which promotes better gliding characteristics confirms increments of earlier studies [4, 3, 6]. In general, the analytic calculations at low AOA provided only fair representations of lift, drag, and moment coefficients, but the predicted trends were in very good agreement, as the data shows.

E. "Louvered" Wing Span Loading

To determine the relative loading of the winglets, the span load distributions were plotted for the louvered configurations at C_L = 0.8 (see Figure 5). In an idealized wing as proposed by Prandtl [16], the span load coefficient would have an elliptical distribution over the span. For the configurations plotted, the baseline actually shows that e = 1.01, which corresponds to the VLM result for full LE suction (for 97% LE suction, e would be about 0.90, a more practical result [15]). The VLM result predicted that e = 1.19–1.30 for the louvered configurations.

These span efficiencies in excess of 1, which have been validated in the literature [3, 7], indicate that a more-efficient distribution of the span loading is possible such that $C_{D,i}$ can be greatly reduced for the same C_L. For individual winglets, this means that the leading winglet is much more highly loaded than the successive ones, and it was found that winglet #1 carried 67% of the loading outboard of the baseline wing tip. Winglets #2 and #3 carried 22% and 11% of the load, respectively.

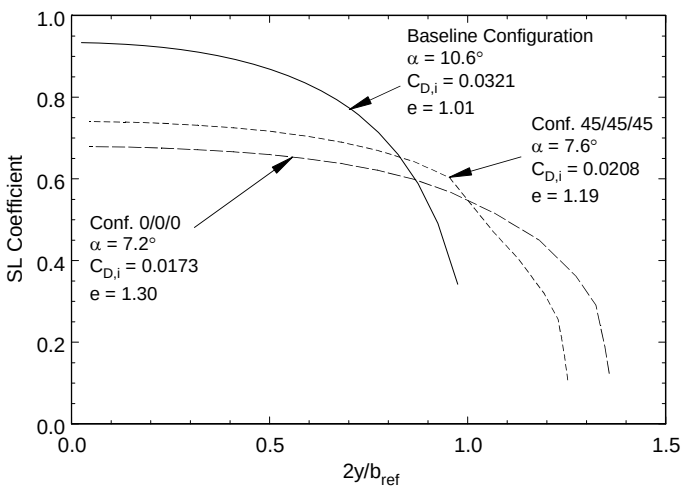

Figure 5. Louvered-wing span load distributions

V. Conclusions

Some general conclusions about the use of multiple winglets were made from the present series of analytic predictions and wind tunnel tests. The airfoil analysis showed that the thinner winglet sections had an 11% lower $C_{L,max}$ and a 50% higher $C_{d,0}$ due to low Reynolds effects. The vortex lattice method provided only fair analytic predictions of the wind tunnel performance, but the predicted trends in lift, drag, and (to a lesser degree) pitching moment were in good agreement with experimental results. However, the primary value of the VLM results was in scrutinizing the spanload distributions of the sectional lift coefficient. This showed that the leading winglet was much more highly loaded than the successive ones, and this affected the overall stall characteristics of the configuration.

The experimental results showed that multiple winglets increased lift and reduced drag. The configurations tested yielded a 41% increase in the lift at equivalent AOA to the baseline wing, and $C_{L,max}$ increased 24%. Measured drag reductions at equivalent lift coefficients were as high as 44%. The cross-over point was observed to be C_L = 0.45, the result of a 32% increase in $C_{D,0}$. Because of the lift increases and the drag reductions, the peak L/D increased by 11%.

From the present study, it can be concluded that multiple winglets can provide increases to lift and L/D at equivalent AOA, while providing decreases in drag at equivalent lift coefficients. This makes multiple winglets appropriate for actively-controlled surfaces for flight-optimized aircraft configurations that depend on high lift and high efficiency, such as present-day UAV configurations. These results call for continued research to study of the effects of the winglets in more detail, in additional dihedral configurations with a focus on optimizing for $C_{L,max}$ and L/D. Furthermore, the effects on lateral and directional stability must be studied to better understand how multiple winglets can be employed to improve the performance of high lift, low speed flight.

VI. References

[1] Fiorino, F. (ed.), 2003, "Southwest 737-700s Earn Winglets," Aviation Week and Space Technology, **158**(25), p. 15.

[2] Proctor, P., 1993, "Winglet Designs to Cut Fuel Burn," Aviation Week and Space Technology, **139**(23), p. 49.

[3] Maughmer, M. D., 2003, "Design of Winglets for High-Performance Sailplanes," J. Aircraft, **40**(6), pp. 1099-1106.

[4] Whitcomb, R. T., 1976, "A Design Approach and Selected Wind-Tunnel Results at High Subsonic Speeds for Wing-Tip Mounted Winglets," NASA Tech. Note D-8260, Nat. Aeronautics and Space Admin.

[5] Chattot, J. J., 2006, "Low Speed Design and Analysis of Wing/Winglet Combinations Including Viscous Effects," J. Aircraft **43**(2), pp. 386-389.

[6] Smith, M. J., Komerath, N., Ames, R., Wong, O., and Pearson J., 2001, "Performance Analysis of a Wing with Multiple Winglets," AIAA paper no. AIAA-2001-2407, American Institute of Aeronautics and Astronautics.

[7] Kroo, I., McMasters, J., and Smith, S. C., 1995, "Highly Nonplanar Lifting Systems," presented at Transportation Beyond 2000: Technologies Needed for Engineering Design, NASA Langley Res. Ctr., Sept. 26-28.

[8] Abbott, I. H. and Von Doenhoff, A. E., 1959, *Theory of Wing Sections Including a Summary of Airfoil Data*, Dover Publications, Mineola, NY, Chaps. 1, 6.

[9] Coleman, H. W. and Steele, W. G., 1995, "Engineering Application of Experimental Uncertainty Analysis," AIAA Journal, **33**(10), pp. 1888-1896.

[10] Barlow, J. B., Rae, W. H., and Pope, A., 1999, *Low-Speed Wind Tunnel Testing*, 3rd ed., John Wiley and Sons, Hoboken, NJ, Chap. 10.

[11] Drela, M., and Youngren, H., 2001, "XFOIL 6.94 User Guide," Aero. and Astro. Engineering, Mass. Inst. of Tech., Cambridge, MA.

[12] Lamar, J. E. and Herbert, H. E., 1982, "Production Version of the Extended NASA-Langley Vortex Lattice FORTRAN Computer Code; Volume I, User's Guide," NASA Tech. Memorandum TM-83303, Nat. Aeronautics and Space Admin.

[13] Lamar, J. E., 2003, discussions of the Vortex Lattice Method involving John Lamar, Pat Bookey, and David Miklosovic at NASA Langley on 29 April 2003.

[14] Miklosovic, D. S., Murray, M. M., Howle, L. E. and Fish, F. E., 2007, "Experimental Evaluation of Sinusoidal Leading Edges," J. Aircraft, **44**(4), pp. 1404-1407.

[15] Samoylovitch, O. and Strelets, D., 2000, "Determination of the Oswald Efficiency Factor at the Aeroplane Design Preliminary Stage," Aircraft Design, **3**(3), pp. 167-174.

[16] Prandtl, L., 1923. "Applications of Modern Hydrodynamics to Aeronautics; Part II: Applications," NACA Report 116 (taken from NASA, 1979, "Classical Aerodynamic Theory," NASA Reference Publication 1050), Nat. Aeronautics and Space Administration).